

# Theoretical investigation of antiferromagnetic skyrmions in a triangular monolayer

Zhaosen Liu<sup>a,1</sup> Manuel dos Santos Dias,<sup>2</sup> and Samir Lounis<sup>2</sup>

<sup>1</sup>*College of Physics and Electronic Engineering,  
Hengyang Normal University, Henghua Road 16, Hengyang 421002, China.*

<sup>2</sup>*Peter Grünberg Institut and Institute for Advanced Simulation,  
Forschungszentrum Jülich & JARA, 52425 Jülich, Germany.*

## Abstract

The chiral spin textures of a two-dimensional (2D) triangular system, where both antiferromagnetic (AF) Heisenberg exchange and chiral Dzyaloshinsky-Moriya interactions co-exist, are investigated numerically with an optimized quantum Monte Carlo method based on mean-field theory. We find that: helical, skyrmionic and vortical AF crystals can be formed when an external magnetic field is applied perpendicular to the 2D monolayer; the sizes of these skyrmions and vortices change abruptly at several critical points of the external magnetic field; each of these AF crystals can be decomposed into three periodical ferromagnetic (FM) sublattices. The quantum ingredient implemented into the theoretical framework helps to track the existence of AF skyrmion lattices down to low temperatures.

PACS numbers: 73.63.Bd, 75.10.Jm 75.40.Mg, 75.75.-c

---

<sup>a</sup> Email: liuzhsnj@yahoo.com

Keywords: Optimized Quantum Monte Carlo, Antiferromagnetic Skyrmionic Lattice, Frustration

## I. INTRODUCTION

Skyrmions in ferromagnetic materials have been intensely studied in recent years.<sup>1–10</sup> Their small size, in a range of  $1\text{ nm} \sim 100\text{ nm}$ , and the very weak electronic current, around  $10^6\text{ Am}^{-2}$ , required to drive them to motion,<sup>11</sup> make them ideal candidates in future data storage and racetrack memory devices. Unfortunately, the Magnus force,<sup>12–14</sup> that acts transversely on the ferromagnetic (FM) skyrmions by the applied electric current, eventually pushes them off the nano-track edge, which greatly hinders their applications in the aforementioned memory devices.<sup>15</sup>

In contrast, an antiferromagnetic (AF) skyrmion in a square lattice can be decomposed into two almost identical FM sublattices. Thus, the Magnus forces acting on the two FM sublattices can be completely cancelled,<sup>16</sup> so that the AF skyrmion can move much faster straightly along the direction of the applied electric current.<sup>16,17</sup>

AF skyrmions have been investigated theoretically in 2D square and triangular antiferromagnets.<sup>18–20</sup> In their Monte Carlo study, Keesman and his colleagues discovered that an isolated skyrmion can be stabilized by a strong external magnetic field at nonzero temperatures, but only in a very tiny finite-sized  $8 \times 8$  square antiferromagnet.<sup>20</sup> For triangular lattices, Rosales et al.<sup>19</sup> observed with classical Monte Carlo (CMC) simulations that when AF Heisenberg exchange (HE) and Dzyaloshinsky-Moriya (DM) interactions co-exist, AF skyrmionic lattices can be induced by an external magnetic field applied normal to the lattice plane in a very low temperature range. However, they found no evidence of AF skyrmion lattice (SL) formation in the AF chiral square lattice. The latter aspect was addressed by one of us<sup>28</sup> utilizing a quantum simulative method, namely the SCA approach, where a self-consistent algorithm is used in the frame of quantum theory.<sup>21–29</sup> It was found that both Bloch and Néel types AF SLs could be induced in a 2D lattice of square crystal structure by a very strong external magnetic field exerted normal to the monolayer plane.<sup>28</sup> We expect that quantum effects, missing in CMC simulations, to be important in AF materials, which motivates the current study by reinvestigating AF SLs formed in the 2D triangular lattices with a method built upon quantum theory.

We utilize here an optimized quantum Monte Carlo (OQMC) method based on a mean-field approach. The Metropolis algorithm is employed, and a simple trick is adopted to improve the computational efficiency. Astonishingly, by using this method we are able to plot, for examples, the well periodic and symmetric AF vortical lattices (VLs), AF skyrmionic lattices (SLs) of both Bloch and Néel types, which can appear at any temperatures in 2D AF chiral magnets, just with the computational results obtained from the last iteration. In contrast, if CMC method is applied to calculate a spin configuration at a finite temperature, averages must be made over thousands of last iterations.

Using the OQMC method, we simulate and investigate in detail the chiral spin textures of a 2D triangular system where the AF HE and chiral DM interactions are both present. Consequently, we find that, within an external magnetic field applied perpendicular to the 2D monolayer, AF HLs (helical lattices), SLs and VLs can be induced at much higher temperatures than predicted by previous authors with CMC simulations;<sup>19</sup> the SL states prevail in a broad  $T - H$  phase area; the sizes of the skyrmions and vortices formed in the spin crystals or lattices changes abruptly when modifying the external magnetic field; each of these AF SL and VL can be decomposed into three FM sublattices that are in fact FM SLs or FM VL, respectively. To check the accuracy of the results obtained with the OQMC method, we carry out simulations using the SCA approach for a particular case with a fixed field strength, and find the resulting AF skyrmionic lattices from both theoretical approaches to be identical.

## II. THE QUANTUM MODEL AND COMPUTATIONAL ALGORITHM

The two-dimensional triangular spin-lattice is considered to be in the  $xy$ -plane, and its corresponding Hamiltonian can be expressed as

$$\mathcal{H} = -\frac{1}{2} \sum_{i,j} \left[ \mathcal{J}_{ij} \vec{S}_i \cdot \vec{S}_j - \vec{D}_{ij} \cdot (\vec{S}_i \times \vec{S}_j) \right] - K_A \sum_i \left( \vec{S}_i \cdot \hat{n} \right)^2 - \vec{H} \cdot \sum_i \vec{S}_i. \quad (1)$$

Here, the first two terms represent the HE and DM interactions between a pair of spins at the  $i$ -th and  $j$ -th lattice sites, respectively. In practice, we restrict the interactions to the nearest neighboring spins. The third term stands for the uniaxial magnetic anisotropy assumed to be normal to the 2D monolayer, which is usually termed as the perpendicular magnetic anisotropy (PMA), and the last one denotes the Zeeman energy of the magnetic system placed in an external

magnetic field. The strengths of the two-spin HE, DM and single-spin PMA interactions are  $\mathcal{J}_{ij}$ ,  $\vec{D}_{ij}$ ,  $K_A$ , respectively. If  $\vec{D}_{ij}$  is along the  $\vec{r}_{ij}$  direction (the vector  $\vec{r}_{ij}$  connecting both spin sites), the induced skyrmion is of Bloch-type; whereas if  $\vec{D}_{ij}$  lies in the film plane and is perpendicular to  $\vec{r}_{ij}$ , the skyrmion is of Néel-type.

In light of quantum theory, the spins appearing in Eq.(1) are quantum operators,<sup>21–29</sup> rather than classical vectors. When  $S = 1$  as it is assumed in the present work, the matrices of the three spin components are:

$$S_x = \frac{1}{2} \begin{pmatrix} 0 & \sqrt{2} & 0 \\ \sqrt{2} & 0 & \sqrt{2} \\ 0 & \sqrt{2} & 0 \end{pmatrix}, S_y = \frac{1}{2i} \begin{pmatrix} 0 & \sqrt{2} & 0 \\ -\sqrt{2} & 0 & -\sqrt{2} \\ 0 & \sqrt{2} & 0 \end{pmatrix}, S_z = \begin{pmatrix} 1 & 0 & 0 \\ 0 & 0 & 0 \\ 0 & 0 & -1 \end{pmatrix}, \quad (2)$$

respectively, in the Heisenberg representation. The thermal expectation value of a physical observable  $A$  at temperature  $T$  can be evaluated with

$$\langle A \rangle = \frac{\text{Tr} [\hat{A} \exp(\beta \mathcal{H}_i)]}{\text{Tr} [\exp(\beta \mathcal{H}_i)]}, \quad (3)$$

where  $\hat{A}$  is the operator of the observable  $A$ , and  $\beta = -1/k_B T$ .

When the quantum Monte Carlo (QMC) method was proposed, Metropolis algorithm was also conventionally employed.<sup>23,27</sup> That is, in every simulation step, a spin  $\vec{S}_i$  is randomly selected from the considered magnetic system, then rotated randomly within a narrow spatial cone. Afterwards, a random number  $r$  is generated to compare with  $p = \exp(-\Delta E_i/k_B T)$ , where  $\Delta E_i$  is the energy change caused by the rotation. If  $r \leq p$ , the operation is accepted, otherwise discarded. All simulations are started from random magnetic configurations above the magnetic transition temperatures, then carried out stepwise down to very low temperatures with a reducing step  $\Delta T < 0$ .

A simple trick has been taken to optimize the QMC method: Once the rotated state of  $\vec{S}_i$  is accepted, the states of its neighboring spins have to be updated immediately, since their states are also affected by the operation. Otherwise, errors in the total energy of the magnetic system will be accumulated, so that the computational program may converge to an incorrect spin configuration.

The above technique taken to optimize QMC method seems very easy and simple. However, it has been proved to be very effective, leading to quick convergence of the simulations. More specifically, OMQC method makes it possible for the computational results obtained in the final iteration after convergency to accurately describe the complicated and detailed spin textures of

considered magnetic system at all temperatures. For instance, with such results we are able to depict well symmetric and periodic FM and AF SkLs of the Bloch- and Néel-types in a broad  $T - H$  phase area in 2D magnetic systems.

### III. COMPUTATIONAL RESULTS

Each lattice site of the AF monolayer is considered to be occupied by an  $S = 1$  spin, both HE and DM interactions are limited to the nearest neighboring spins, and their strengths assigned to  $\mathcal{J}_{ij} = \mathcal{J} = -1$ ,  $D_{ij} = D = 1$ , respectively. That is, all parameters and other physical quantities are scaled with  $|\mathcal{J}|$ . Since these two interactions are comparable in magnitude, the ground state of the magnetic system is neither simply antiferromagnetic nor vortical. To generate isolated skyrmions or SLs, an external magnetic field  $\vec{H}$  that is normal to the monolayer has to be considered.<sup>19,20</sup> A  $30 \times 30$  square lattice is chosen in most our simulations, and periodical boundary conditions are imposed to mimic the infinite size of the 2D monolayer and to facilitate formations of chiral spin lattices.

#### A. Phase Diagram

From our simulated results, we find that well symmetric and periodical AF SLs can be generated when the external magnetic field falls in a wide range  $1 \leq H \leq 7.4$ , as shown in the phase diagram plotted in Figure 1(a). To get this diagram, the applied magnetic field strength is varied from 0.4 to 7.8; and in an external field of fixed strength, the simulation is initiated from a random spin configuration in the paramagnetic phase, then temperature is lowered with a reducing step  $\Delta T = -0.1$  or  $-0.05$ .

In Figure 1(a),  $T_{HL}$ ,  $T_{SL}$ ,  $T_{SV}$  represent the transition temperatures when the magnetic system condenses to the AF helical, skyrmionic and vortical lattices, respectively. Therefore, the area below the curve  $T_\alpha$  and above the curve  $T_\beta$  is in the  $\alpha$  phase; whereas the region below the lowest curve  $T_\gamma$  is in the  $\gamma$  phase. For example, as  $6.0 \leq H \leq 7.4$ , the area between the  $T_{VL}$  and  $T_{SL}$  curves is the VL phase, whereas the region below the  $T_{SL}$  curve is in the SL phase; while in the field range  $1.0 \leq H \leq 1.6$ , the area between the  $T_{SL}$  and  $T_{HL}$  curves is the SL phase, whereas the region below the  $T_{HL}$  curve is the HL phase. In a wide field range  $1.8 \leq H \leq 5.8$ , only AF SLs

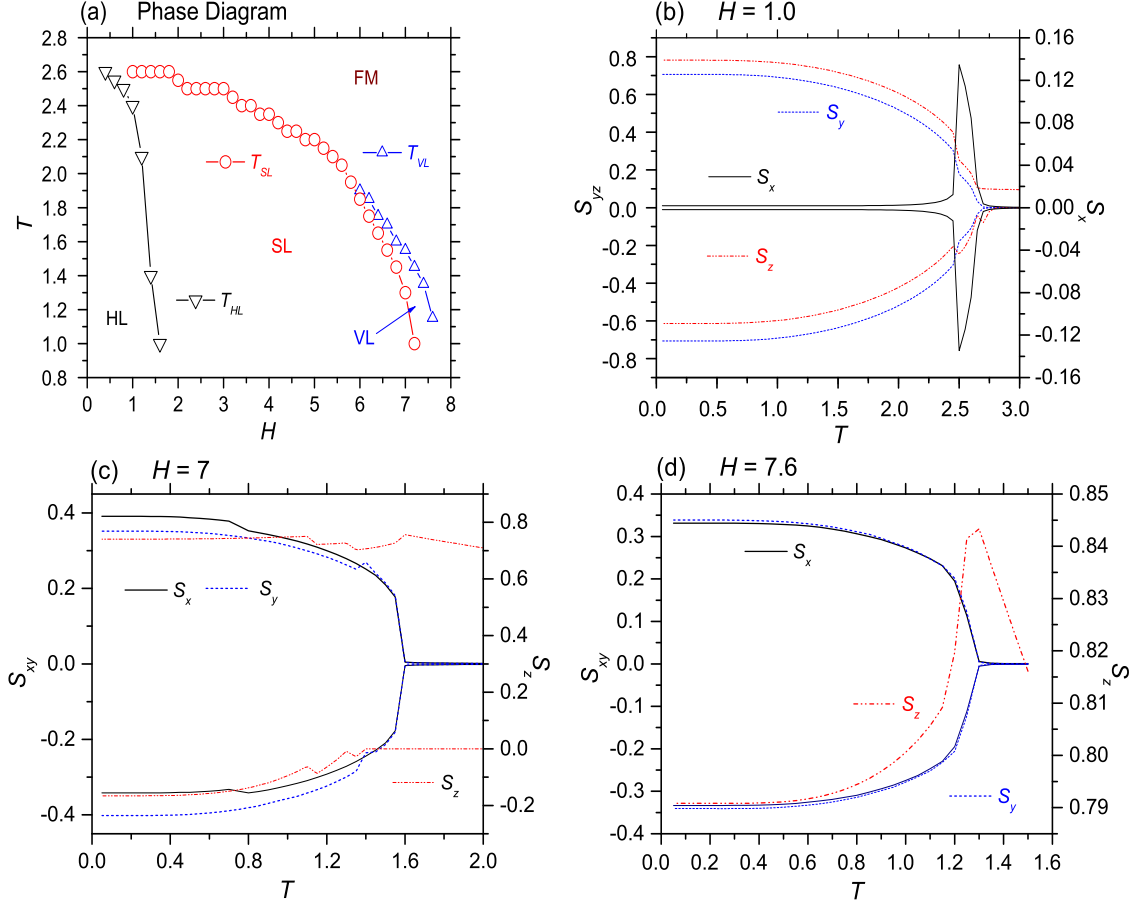


FIG. 1. Calculated phase diagram (a),  $S_x$ ,  $S_y$  and  $S_z$  curves for  $H = 1.0$  scaled with  $\mathcal{J}$  ( $S_x$  is displayed in a different scale) (b),  $H = 7$  (c), and  $H = 7.6$  (d), versus temperature.

appear below the  $T_{SL}$  curve; while for  $0.4 \leq H \leq 0.8$ , only HL states prevail below the  $T_{HL}$  curve. As expected, at high temperatures the system is completely polarized by the applied magnetic field and becomes ferromagnetic.

Figures 1(b,c,d) display the  $\langle S_x \rangle$ ,  $\langle S_y \rangle$  and  $\langle S_z \rangle$  curves of the AF system when it is placed in external magnetic fields of different strengths. In the first case shown in Figure 1(b),  $H = 1.0$  which is in the unit of  $\mathcal{J}$ . Please note here that  $\langle S_x \rangle$  and  $\langle S_y \rangle$  are displayed in different scales. Above  $T = 2.8$ , the spins are completely polarized to the  $z$ -direction by the external magnetic field. When temperature drops to  $T = 2.6$  and  $2.5$ , the positive and negative branches of  $\langle S_x \rangle$  and  $\langle S_y \rangle$ , though very weak, are comparable in magnitude, thus AF SLs can be generated. However, as temperature drops further, the magnitudes of  $\langle S_x \rangle$  and  $\langle S_y \rangle$  differ considerably, while those of  $\langle S_y \rangle$  and  $\langle S_z \rangle$  are comparable, so that vertical AF HL state dominates the whole low temperature

range.

In the second case shown in Figure 1(c),  $H = 7$ . As  $T > 1.6$ , only  $\langle S_z \rangle$  is sizable. That is, the whole system is almost completely polarized by this strong external magnetic field. Below  $T = 1.6$ , the positive and negative branches of both  $\langle S_x \rangle$  and  $\langle S_y \rangle$  grow gradually with decreasing temperature, and later become comparable in magnitude, but they are shifted relatively with each other in the vertical direction, so that VLs can be formed within temperature range  $1.55 \geq T > 1.3$ , whereas SLs are induced below  $T_{SL} = 1.3$ .

It is easy to understand that, when  $H = 7.6$  as shown in Figure 1(d), only VL can be observed below  $T_{VL} = 1.15$ , since all spins have been rotated by the external magnetic field toward the  $z$ -direction. Especially, when  $H$  is increased to 7.6, the size of each vortex suddenly grows, and we have to use a  $60 \times 60$  lattice to generate these VL structures.

## B. FM Sublattices of Helical, Skyrmionic and Vortical Lattices

The co-presence of AF HE and DM interactions gives rise to very complicated spin configurations, so that the AF spin lattices, though they are well periodical and symmetric, look quite puzzling if the  $xy$  projection and  $z$ -contour of such a spin crystal are plotted together. Fortunately, each of these spin textures can be decomposed into three FM sublattices.

Figures 2 (a-d) display the  $xy$ -projection and the three FM sublattices of the helix obtained at  $H = 0.4$  and  $T = 0.1$ . The helical lattice is vertical, i.e., the  $x$ -component of each spin is negligible, whereas other two components are dominant. In each sublattice, the periodical wavelength  $\lambda = 6a$  in the  $x$ -direction; and the three sub-HLs are staggered with each other in the same direction.

Figure 3 displays the  $xy$ -projection and the three sublattices of an AF SL calculated at  $H = 7$ ,  $T = 0.05$ . In Figure 3(a) we can find that AF SL shows a hexagonal pattern, so are its three FM sublattices. But as displayed in Figure 3(b-d), the latter three have been rotated about  $\pi/4$  clockwise. Interestingly, each of the three sublattices is an FM SL consisting of 12 FM skyrmions inside the  $30 \times 30$  lattice. All these FM skyrmions are left-handed since  $D/\mathcal{J} < 0$ . The three FM SLs are staggered with each other, the skyrmions in these sublattices are elongated along slightly different directions, so that the FM sublattices are not identical. In each SL, the spins in the interstitial region, which has a size comparable to that of the skyrmion, do not form vortex, and some of the neighboring spins align approximately antiparallel owing to spin frustration. The spin

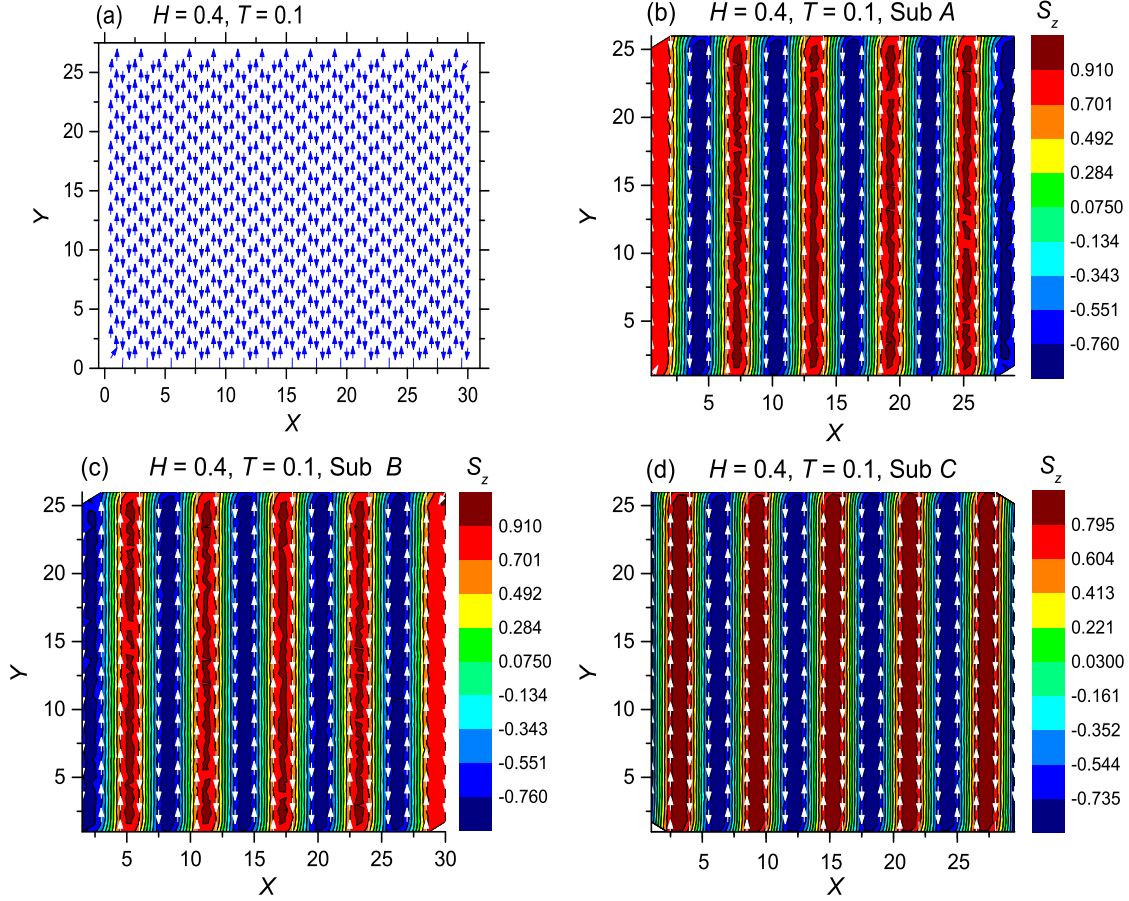


FIG. 2. Calculated  $xy$ -projection (a), and three FM sublattices (b,c,d) of the AF spiral when  $H = 0.4$  and  $T = 0.1$ . Sub A, B and C are the three sublattices.

textures in these interstitial areas seem quite 'random' in the  $xy$ -plane, but they are astonishingly still periodic in each FM sublattice. These 'disordered' textures look completely different from those obtained in CMC simulations,<sup>19</sup> and as a result, give rise to increased magnetic entropy,  $S_M$ , and reduced total free energy,  $F$ , of the whole system, since  $F = E - TS_M$ , so that the AF SLs are better stabilized.

When  $H = 7.6$  as shown in Figure 4, the  $z$ -components of all spins become positive, so only VL can be formed below  $T_{VL} = 1.15$ . The AF vortices form regular hexagonal VL, whose three FM sublattices show the same pattern but all rotated around the  $z$ -axis. More interestingly, the size of each vortex increases suddenly, so that we have to use a  $60 \times 60$  lattice to produce the VL texture. For comparison, a  $30 \times 30$  portion is displayed in Figure 4, therein 6 FM vortices are observed in each FM sublattice. Once again, the three sublattices are FM VLs, they are nonidentical, and



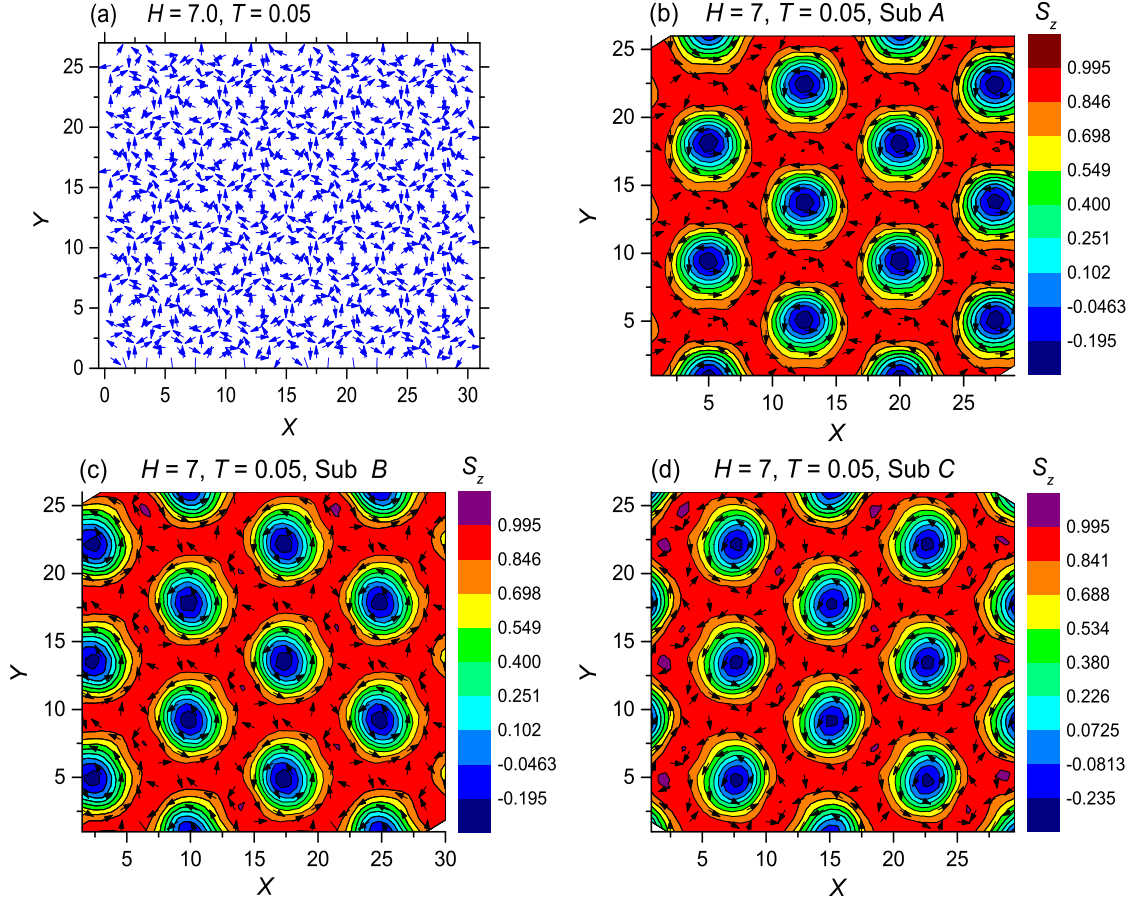


FIG. 3. Calculated  $xy$ -projection (a) and three FM sublattices (b,c,d) of the AF SL when  $H = 7$ ,  $T = 0.05$ .

staggered with each other. Nevertheless, each FM VL shows excellent periodicity and symmetry.

When  $H$  is reduced to 6.6, each skyrmion in the AF SL shrinks considerably. So we can find in Figure 5, obtained at  $H = 5$ ,  $T = 2$ , each FM SL contains 20 skyrmions in the rotated HCP pattern. In addition, in the (a) sub-figure, two inclined spin strips emerge with their lower ends terminating around  $x = 1$  and  $15$ , respectively. The two strips do spoil the periodicity of the AF SL shown in the first sub-figure, however, they have seemly no evident effects upon the periodicity and symmetry of the three FM sublattices.

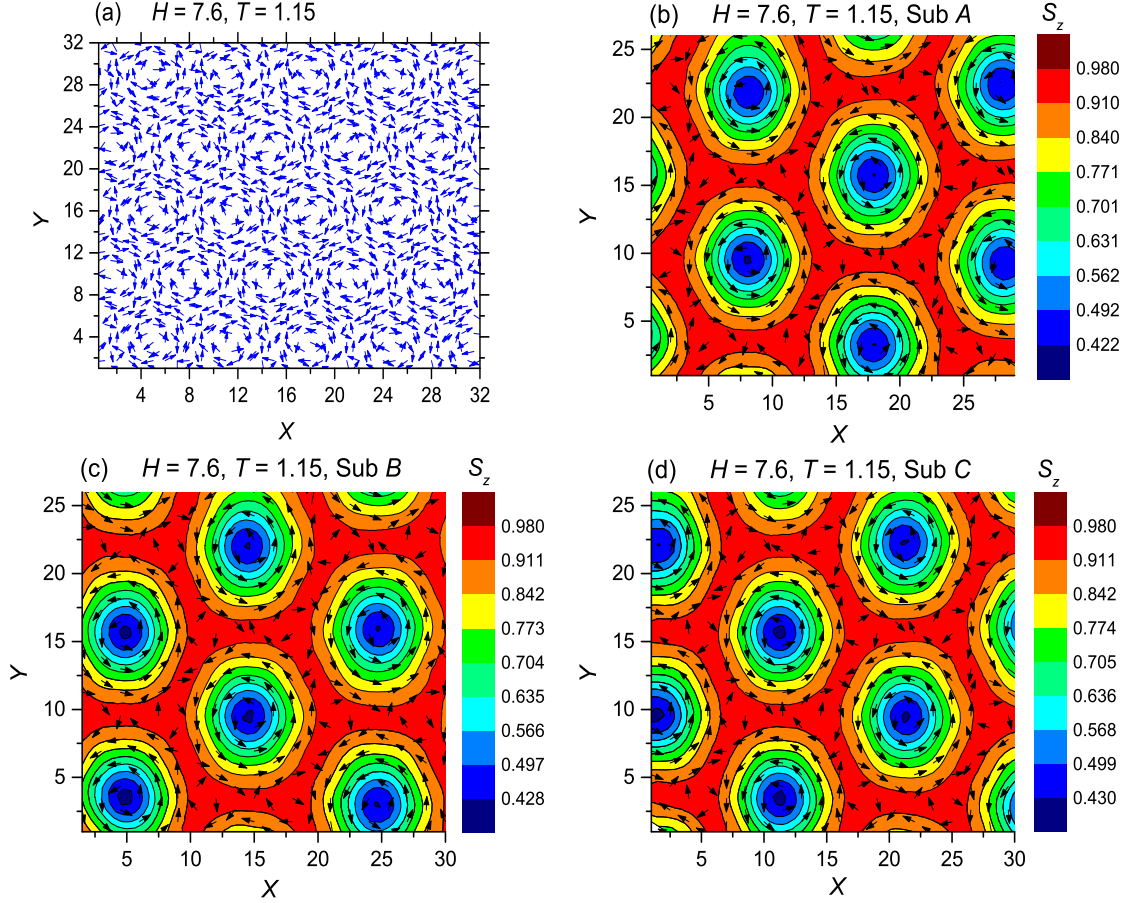


FIG. 4. Calculated  $xy$ -projection (a), and three FM sublattices (b,c,d) of the AF SL as  $H = 7.6$ ,  $T = 1.15$ .

### C. Distribution of Topological Charge Density of Each Sublattice

For a discretized model, the topological charge can be expressed with<sup>19,30,31</sup>

$$\chi_Q = \frac{1}{4\pi} \left\{ \sum_{\vec{r}_i} A_{\vec{r}_i}^{(12)} \text{sign}[\chi_{L,\vec{r}_i}^{(12)}] + A_{\vec{r}_i}^{(34)} \text{sign}[\chi_{L,\vec{r}_i}^{(34)}] \right\}, \quad (4)$$

where  $A_{\vec{r}_i}^{(ab)} = ||(\vec{S}_{\vec{r}_a} - \vec{S}_{\vec{r}_i}) \times (\vec{S}_{\vec{r}_b} - \vec{S}_{\vec{r}_i})||/2$  is the local area of the surface spanned by three spins at  $\vec{r}_i$ ,  $\vec{r}_a$  and  $\vec{r}_b$  of an elementary triangle,  $\chi_{L,\vec{r}_i}^{(ab)} = \vec{S}_{\vec{r}_i} \cdot (\vec{S}_{\vec{r}_a} \times \vec{S}_{\vec{r}_b})$  denotes the local chirality, and  $\vec{r}_i, \vec{r}_1 \sim \vec{r}_4$  are the sites involved in the calculation of  $\chi_Q$  as described in Rosales et al.'s article.<sup>19</sup>

Using above formulas, we find that the calculated topological charge density of each sublattice also forms periodical crystals, as shown in Figures 6 ~ 7(b,c,d), that are obtained at  $H = 7$ ,  $T = 0.05$ , and  $H = 5$ ,  $T = 2$ , respectively. Here, the rainbow-like contour denotes the topological charge

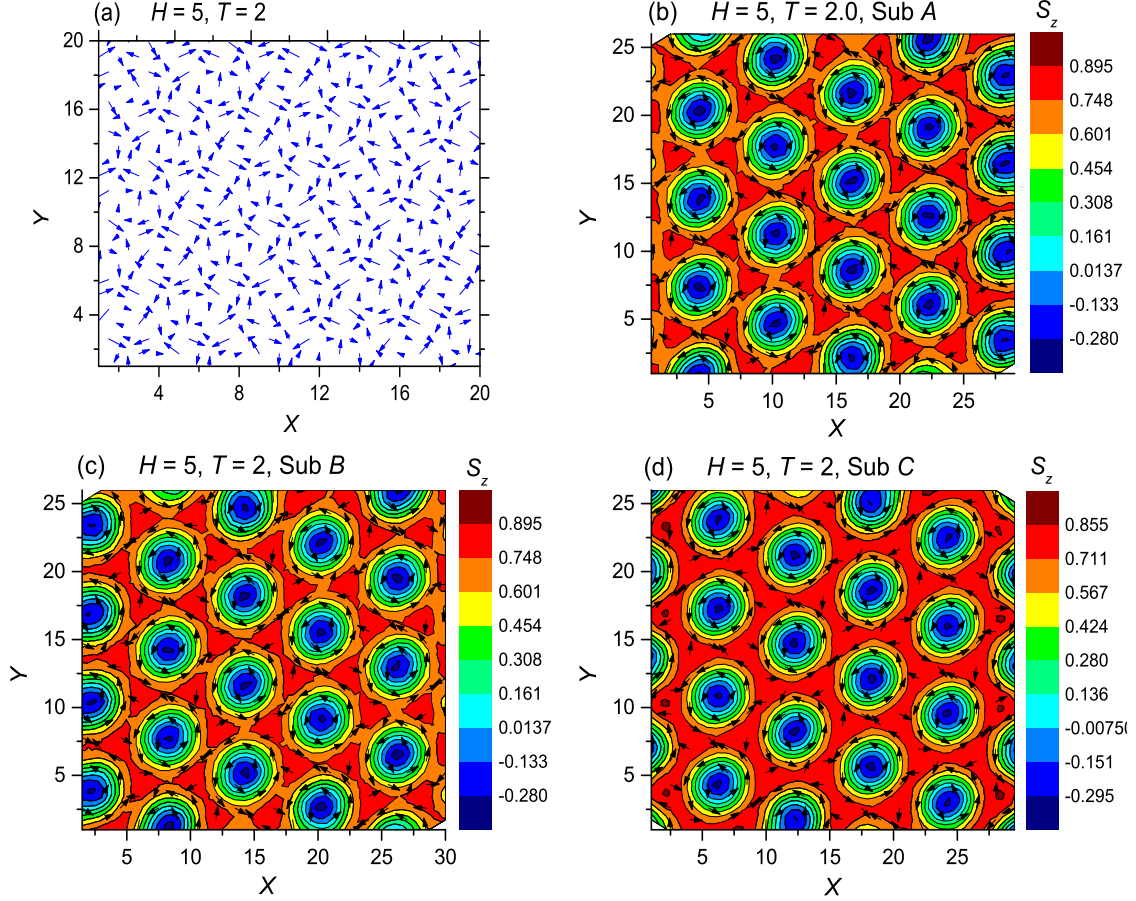


FIG. 5. Calculated  $xy$ -projection (a), and three FM sublattices (b,c,d) of the AFM SkL as  $H = 5$ ,  $T = 2$ .

density,  $\rho$ , at the lattice sites, and the arrows show the  $xy$  projections of the FM spin sublattice of the AF SL. Clearly, each charge density crystal is almost exactly identical with the corresponding FM spin sublattice. The three  $\rho$  sublattices of an AF SL differ from each other, and we observe much densely packed  $\rho$  unit cells in Figure 7(b,c,d).

In Figure 6(a) and Figure 7(a), the  $\chi_Q$  curves are plotted versus changing temperature. There,  $\gamma$  represents the ratio of the spin number of those with negative  $\langle S_z \rangle$  to the whole spin number. In the first case,  $H = 7$ ,  $T_{VL} = 1.55$  and  $T_{SL} = 1.3$ . So above  $T_{VL}$ ,  $\gamma$  and  $\chi_Q^{A,B,C}$  are all equal to zero. From  $T_{SL}$  down to  $T = 1.10$ ,  $\gamma$  increases from 0.0414 to 0.0784, then remains unchanged until  $T = 0.05$ . At all temperatures, less than 8% spins align opposite to the applied magnetic field, so the chiral spin textures are far away from fully 'skyrmionic'. Carefully inspecting each FM sublattice, we can see that the spin texture in each interstitial region exhibits completely different

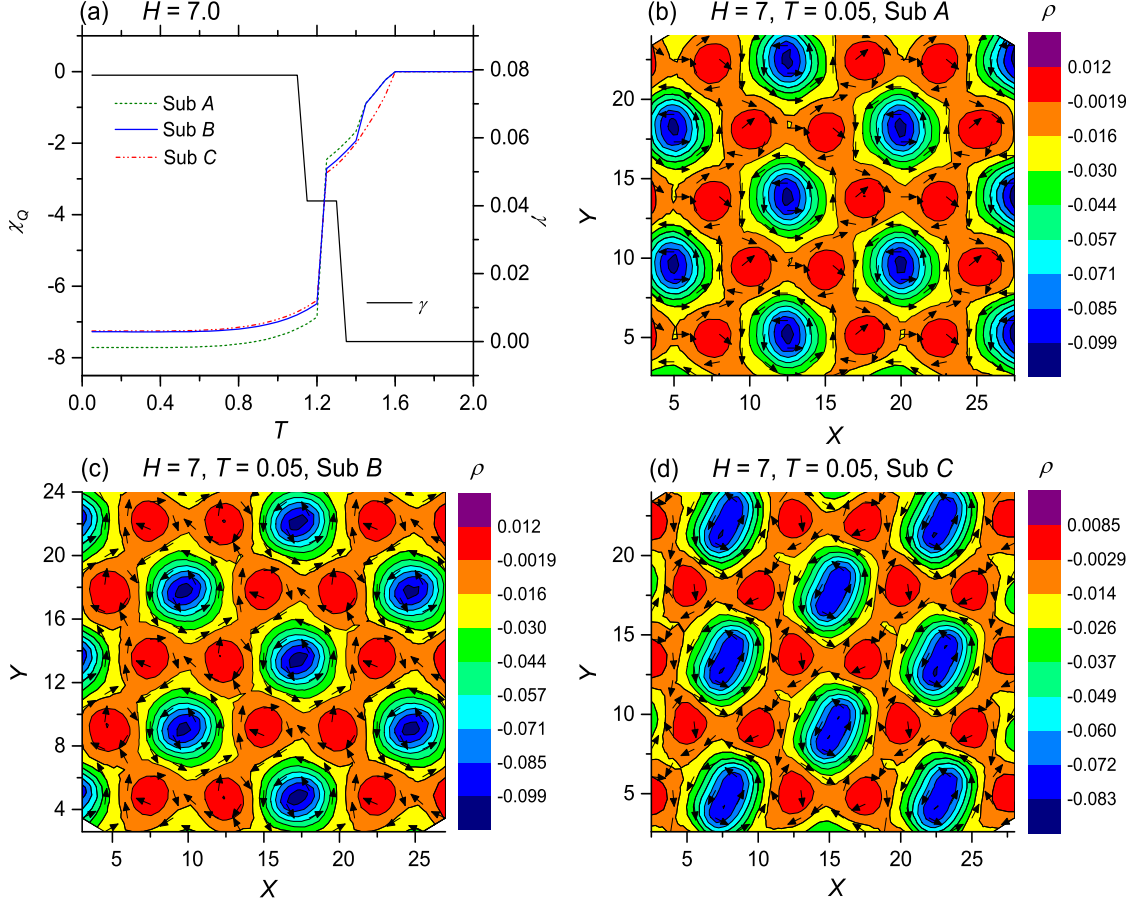


FIG. 6. Total topological charges (a), and charge density distributions of the three FM sublattices (b,c,d), of the AF SL calculated at  $H = 7$ ,  $T = 0.05$ .

features from the surrounding skyrmions, and the two sorts of spin textures are entangled together. Thus, at  $H = 7$  and  $T = 0.05$ , the averaged topological charge per skyrmionic complex, consisting of one skyrmion and its surrounding area,  $Q_{av} \in (-0.643, -0.606)$ . In the second case,  $H = 5$  and  $T = 2.0$ . Though the three spin sublattices are FM SLs,  $\gamma$  is around 0.166, the SLs are also not fully skyrmionic yet, thus  $Q_{av} \in (-0.588, -0.581)$ .

#### D. Spin Structure Factors of the Helical, Skyrmionic and Vortical Lattices

To characterize the spin-textures, the static spin structure factors in the reciprocal space have to be calculated, of which the out and in plane components  $S_{\perp}(q)$  and  $S_{\parallel}(q)$  are defined as

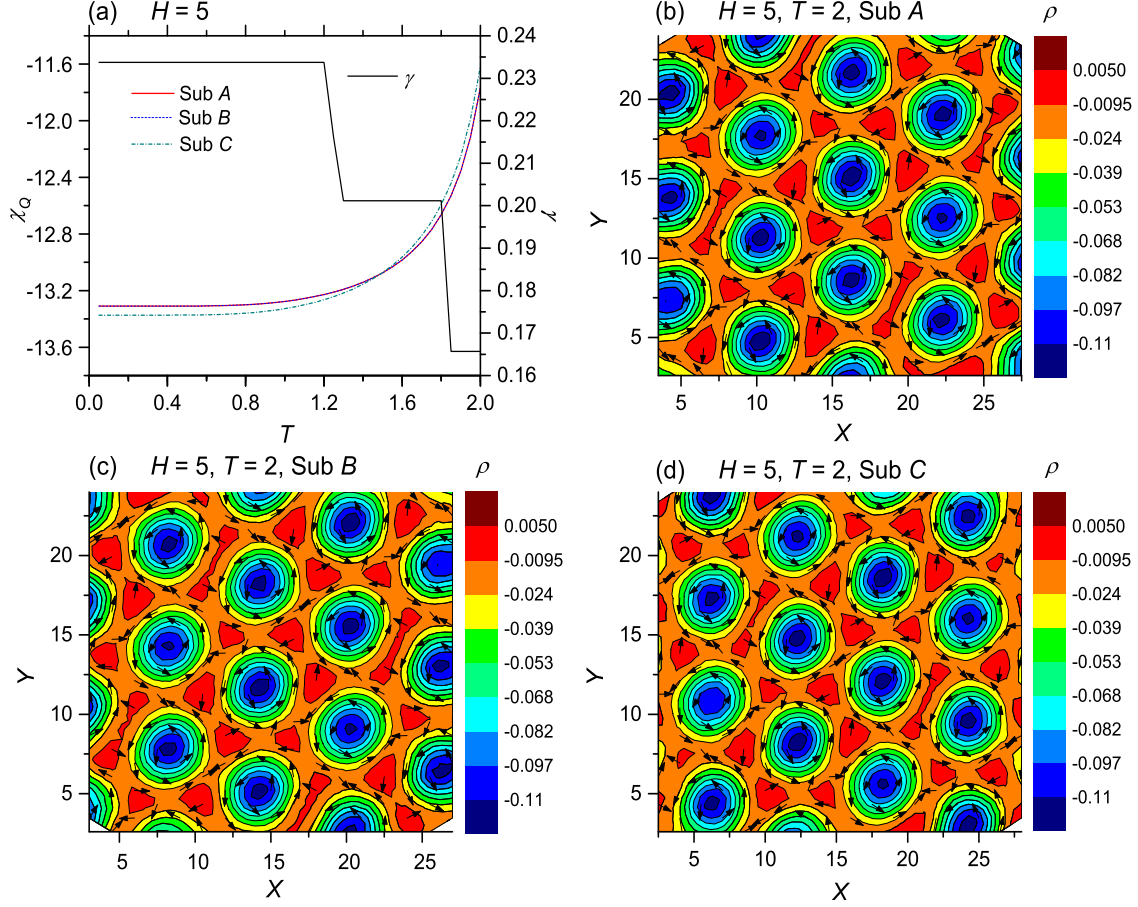


FIG. 7. Total topological charges (a), and charge density distributions of the three FM sublattices (b,c,d), of the AF SL calculated at  $H = 5, T = 2$ .

$$\begin{aligned}
 S_{\perp}(q) &= \frac{1}{N} \left( \left| \sum_{\vec{r}_i} S_{\vec{r}_i}^x e^{-i\vec{q} \cdot \vec{r}_i} \right|^2 + \left| \sum_{\vec{r}_i} S_{\vec{r}_i}^y e^{-i\vec{q} \cdot \vec{r}_i} \right|^2 \right), \\
 S_{//}(q) &= \frac{1}{N} \left( \left| \sum_{\vec{r}_i} S_{\vec{r}_i}^z e^{-i\vec{q} \cdot \vec{r}_i} \right|^2 \right),
 \end{aligned} \tag{5}$$

respectively.

Figure 8(a ~ f) displays the intensity of the spin texture factor for the AF HL, AF SL and AF VL, respectively. The colored spectral band on the right side of each sub-figure shows the scaled intensity of the spin texture factor. In both Figure 8(a) and(b), the two spectra look the same, those bright spots form square pattern out of the blue background. Though the skyrmions and vortices shown in Figure 3 and 4 respectively are of very different sizes, the brightest points of

$S_{\perp}(q)$  in Figure 8(d,f) exhibit the same hexagonal pattern if other less strong points are neglected. Large differences are detected in Figure 8(c) and (e), where the  $S_{//}(q)$  spectra of the AF SL and VL are displayed. However, each of them is symmetric about its center, and has a quite large hexagon in the central region of the reciprocal 2D space.

#### IV. COMPARISON WITH SCA METHOD

From now on, other simulated results will be displayed in the appendixes for compactness.

To check our results, we repeat the simulations by means of the SCA method.<sup>21–24,26–29</sup> Astonishingly, as  $H = 7$ , the  $xy$ -projections of the AF SLs obtained at different temperatures with the two methods, when plotted together, overlap with each other exactly, except for  $T = T_{VL} = 1.55$ , where the system starts to condense to the VL state, only at a few sites the spins align in slightly different directions. Figure S1 shows an example at a very low temperature,  $T = 0.05$ , in comparison with the results, that are shown in Figure 3 and calculated with the same set of parameters using the OQMC method. No doubt, if the  $A$ ,  $B$  and  $C$  FM sublattices obtained with the two quantum approaches are plot together correspondingly, every pair will overlap with each other almost exactly.

For the same purpose, the calculated total topological charges versus varying temperature as  $H = 7$ , and charge density textures of the  $A$ ,  $B$  and  $C$  FM sublattices of the AF SL obtained at  $T = 0.05$  with the SCA approach, are displayed in Figure S2. When compared with the four pictures displayed in Figure 6, that are obtained with the OQMC method using the same set of parameters, we can hardly detect any disparity in each pair of the corresponding sub-figures.

#### V. CONCLUSIONS AND DISCUSSION

In this work, we have investigated spin textures of a 2D triangular lattice in the presence of AF HE and chiral DM interactions with a quantum Monte Carlo method optimized recently. It is observed that within an external magnetic field applied normal to the 2D plane, well periodic and symmetric AF helical, skyrmionic and vortical lattices can be generated at temperatures higher than those predicted by previous authors;<sup>19</sup> the AF SL states prevail in a broad  $T - H$  region in the phase diagram; the sizes of skyrmions and vortices change discontinuously at a few critical



points of the applied magnetic field; each of these AF periodical SLs and VLs can be decomposed into three FM sublattices; and the topological charge density of each FM sublattices of an AF SL also forms crystal which coincides with that FM SL almost exactly; the intensity of spin structure factor of each AF lattice varies in a very broad range in the 2D reciprocal space, where the bright points in the  $q_x \sim q_y$  plane form symmetric patterns, but most points have very low intensity, which are connected continuously to form a blue background.

In fact, we have performed simulations with different  $D/|\mathcal{J}|$  ratios, but only the results for  $D/|\mathcal{J}| = 1$  are presented in this manuscript for compactness. In general, the larger the ratio, the smaller periodicity of the AF SL; and our calculated  $T_{VL}$  and  $T_{SL}$  are usually several times larger than those estimated by the CMC method.<sup>19</sup> For instance, when  $D/\mathcal{J} = -0.5$  and  $H = 2.4$ , our calculated  $T_{SL} \approx 2.0$ , that is about 6 time larger than the value obtained from the CMC simulations.<sup>19</sup>

According to the Metropolis algorithm, in every computing step, a random number  $r_i$  must be generated and compared with  $p_i = e^{-\Delta E_i/k_B T}$ , where  $\Delta E_i$  denotes the energy change caused by rotating spin  $\vec{S}_i$ . Near the transition temperature,  $|\Delta E_i|/k_B T \ll 1$ . To correctly determine the new state of  $\vec{S}_i$ ,  $\Delta E_i$  must be accurately evaluated. In the system we currently consider, the co-existence of chiral DM and especially AF HE interactions make it very difficult to calculate  $\Delta E_i$  accurately if a classical method is employed, since antiferromagnetic systems are intrinsically 'quantum'. On the other hand, in CMC simulations, thousands of spin configurations after 'convergence' must be taken to calculate the averaged values of the spin vectors to determine the spin textures at a given temperature. Thus, if these spin configurations are not accurately determined, or because of the AF HE and DM interactions, the orientations of any spin can differ greatly or may be nearly opposite in different iterations, so the regular spin textures may be smeared out by averaging over those non-well determined spin configurations and finally become featureless, so that the transition temperature may be considerably underestimated. Or even worse, the AF chiral spin texture existing at very low temperatures can not be detected with the CMC method.

## Acknowledgements

Z.-S. Liu acknowledges Professor Stefan Blügel for helpful discussion, the financial support provided by National Natural Science Foundation of China under grant No. 11274177, and by Peter Grünberg Institut and Institute for Advanced Simulation, Forschungszentrum Jülich, Germany

during the visit in last Summer.

- 
- <sup>1</sup> A. Bogdanov, and A. Huber, Thermodynamically stable magnetic vortex states in magnetic crystals, *J. Magn. Magn. Mater.* 138, 255-269 (1994)
  - <sup>2</sup> A. Bogdanov, and A. Hubert, The stability of vortex-like structures in uniaxial ferromagnets, *J. Magn. Magn. Mater.* 195, 182-192 (1999)
  - <sup>3</sup> A. N. Bogdanov, and U. K. Röβler, Chiral symmetry breaking in magnetic thin films and multilayers, *Phys. Rev. Lett.* 87, 037203 (2001).
  - <sup>4</sup> C. Pappas, E. Lelievre-Berna, P. Falus, P. M. Bentley, E. Moskvina, S. Grigoriev, P. Fouquet, and B. Farago, Chiral paramagnetic skyrmion-like phase in MnSi, *Phys. Rev. Lett.* 102, 197202 (2009).
  - <sup>5</sup> X. Z. Yu, Y. Onose, N. Kanazawa, J. H. Park, J. H. Han, Y. Matsui, N. Nagaosa, and Y. Tokura, Real-space observation of a two-dimensional skyrmion crystal, *Nature* 465, 901-904 (2010).
  - <sup>6</sup> S. Banerjee, J. Rowland, O. Erten, and M. Randeria, Enhanced stability of skyrmions in two-dimensional chiral magnets with Rashba spin-orbit coupling, *Phys. Rev. X* 4, 031045 (2014).
  - <sup>7</sup> S.D., Yi, S. Onoda, N. Nagaosa, and J. H. Han, Skyrmions and anomalous Hall effect in a Dzyaloshinskii-Moriya spiral magnet, *Phys. Rev. B* 80, 054416 (2009).
  - <sup>8</sup> S. Buhbrandt, and L. Fritz, Skyrmion lattice phase in three-dimensional chiral magnets from Monte Carlo simulations, *Phys. Rev. B* 88, 195137 (2013).
  - <sup>9</sup> S. X. Huang, and C. L. Chien, Extended skyrmion phase in epitaxial FeGe(111) thin film, *Phys. Rev. Lett.* 108, 267201 (2012).
  - <sup>10</sup> N. Romming, A. Kubetzka, C. Hanneken, K. von Bergmann, and R. Wiesendanger, Field-dependent size and shape of single magnetic skyrmions, *Phys. Rev. Lett.* 114, 177203 (2015).
  - <sup>11</sup> J. Iwasaki, M. Mochizuki, and N. Nagaosa, Universal current-velocity relation of skyrmion motion in chiral magnets, *Nat. Commun.* 4 1463 (2013).
  - <sup>12</sup> R. Tomasellor, E. Martinez, R. Zivieri, L. Torres, M. Carpentieri, and G. Finocchio, A strategy for the design of skyrmion racetrack memories, *Sci. Rep.* 4, 6784 (2014).
  - <sup>13</sup> K. Everschor, M. Garst, R. A. Duine, and A. Rosch, Current-induced rotational torques in the skyrmion lattice phase of chiral magnets, *Phys. Rev. B* 84, 064401 (2011).
  - <sup>14</sup> I. A. Ado, O. A. Tretiakov, and M. Titov, Microscopic theory of spin-orbit torques in two



- dimensions, *Phys. Rev. B* 95, 094401 (2017).
- <sup>15</sup> A. Fert, V. Cros, and J. Sampaio, Skyrmions on the track, *Nat. Nano.* 8, 152 (2013).
  - <sup>16</sup> J. Barker, and O. A. Tretiakov, Static and dynamical properties of antiferromagnetic skyrmions in the presence of applied current and temperature, *Phys. Rev. Lett.* 116, 147203 (2016).
  - <sup>17</sup> H. Velkov, O. Gomonay, M. Beens, G. Schwiete, A. Brataas, J. Sinova, and R. A. Duine, Phenomenology of current-induced skyrmion motion in antiferromagnets, *New J. Phys.* 18, 075016 (2016).
  - <sup>18</sup> T. Okubo, S. Chung, and H. Kawamura, Multiple-q states and the skyrmion lattice of the triangular-lattice Heisenberg antiferromagnet under magnetic fields, *Phys. Rev. Lett.* 108, 017206 (2012).
  - <sup>19</sup> H. D., Rosales, D. C. Cabra, and P. Pujol, Three-sublattice skyrmion crystal in the antiferromagnetic triangular lattice, *Phys. Rev. B* 92, 214439 (2015)
  - <sup>20</sup> R. Keesman, M. Raaijmakers, A. E. Baerends, G. T. Barkema, and R. A. Duine, Skyrmions in square-lattice antiferromagnets, *Phys. Rev. B* 94, 054402 (2016)
  - <sup>21</sup> Z.-S. Liu, V. Sechovský, and M. Diviš, Magnetism of  $\text{PrAl}_2$  nanoparticle investigated with a quantum simulation model, *J. Phys.: Condens. Matter* 23, 016002 (2011).
  - <sup>22</sup> Z.-S. Liu, V. Sechovský, and M. Diviš, Magnetism of  $\text{DyNi}_2\text{B}_2\text{C}$  nanoparticle investigated with a quantum simulation model, *Phys. Status Solidi B* 249, 202-208 (2012).
  - <sup>23</sup> Z.-S. Liu, V. Sechovský, and M. Diviš, Mutual verification of two new quantum simulation approaches for nanomagnets, *Physica E* 62, (2014) 123-127
  - <sup>24</sup> Z.-S. Liu, and H. Ian, Effects of Dzyaloshinsky-Moriya interaction on magnetism in nanodisks from a self-consistent approach. *J. Nanopart. Res.* 18, 9 (2016).
  - <sup>25</sup> Z.-S. Liu, and H. Ian, Numerical studies on antiferromagnetic skyrmions in nanodisks by means of a new quantum simulation approach, *Chem. Phys. Lett.* 649, 135-140 (2016).
  - <sup>26</sup> Z.-S. Liu, O. Ciftja, and H. Ian, Interplay of Dzyaloshinsky-Moriya and dipole-dipole interactions upon the vortical structures on nanodisks investigated by means of a quantum simulation approach. *Physica E* 90, 13-20 (2017).
  - <sup>27</sup> Z.-S. Liu, O. Ciftja, X.-C. Zhang, Y. Zhou, and H. Ian, Vortical structures for nanomagnetic memory induced by dipole-dipole interaction in monolayer disks, *Superlatt. Microstr.* 117, 495-502 (2018).
  - <sup>28</sup> Z.-S. Liu, and H. Ian, Ferromagnetic sublattices of antiferromagnetic skyrmion crystals formed

- in two-dimensional square lattices, *Superlattices Microstruct.* **126** 25-31 (2019).
- <sup>29</sup> Z.-S. Liu, and H. Ian, A Sum rule of uniaxial anisotropy and external magnetic field for formation of Neel-type skyrmion lattices in two-dimensional ferromagnets, *J. Phys.: Condens. Matter.* **31**, 29 (2019).
- <sup>30</sup> P. W. Anderson and H. Hasegawa, *Phys. Rev.* **100**, 675 (1955)
- <sup>31</sup> K. Ohgushi, S. Murakami, and N. Nagaosa, *Phys. Rev. B* **62**, R6065 (2000)

## Appendix A: Comparison of results: OQMC versus SCA methods

To assess the results obtained with the OQMC method, we have repeated the simulations by means of another quantum approach, namely the SCA method since the self-consistent algorithm is employed there.<sup>21–24,26,27,29</sup> The results obtained with  $\mathcal{J} = -1$ ,  $D = 1$ , and  $H = 7$  are displayed in Figure S1 and S2 in comparison with those depicted in Figure 3 and 6, correspondingly.

The  $xy$ -projections of the AF SLs obtained at different temperatures using the two methods, when plotted together, overlap with each other almost exactly, as shown in Figure S1(a). Just at  $T = T_{VL}$  ( $= 1.55$ ), where the system starts to condense to AF VL state, only a few spins align in different directions. If the  $A$ ,  $B$  and  $C$  FM sublattices obtained with the two quantum approaches are plotted together, every pair of them overlaps with each other almost exactly as well.

In Figure S2 and Figure 6, the curves of the total topological charges versus changing temperature, the charge density distributions of the  $A$ ,  $B$  and  $C$  FM sublattices of the AF SL at  $T = 0.05$ , that are calculated with the two methods, show no disparity.

## Appendix B: Néel-Type AF SL Simulated with OQMC Method

By assigning  $\mathcal{J} = -1$ ,  $D = 1$ , and  $H = 7$  which is perpendicular to the 2D antiferromagnet, OQMC simulations are started from a paramagnetic state, then carried out down to a very low temperature,  $T = 0.05$ . Now,  $\vec{D}$  is assumed to be in-plane and normal to  $\vec{r}_{ij}$ , so the induced AF SL shown in Figure S3 and S4 are of Néel-type.

As shown in these two figures, this AF SL can also be decomposed to three FM SL, each of them contains 12 FM skyrmions in the  $30 \times 30$  lattice, and the topological charge density of each FM sublattice forms a periodical crystal of the same pattern as the spin sublattice.

In comparison with the results shown in Figure 3 and 6, we can see that the two types of AF SLs obtained with the same set of parameters exhibit very similar characteristics. So the AF SLs of the Bloch and Néel types form a dual pair.

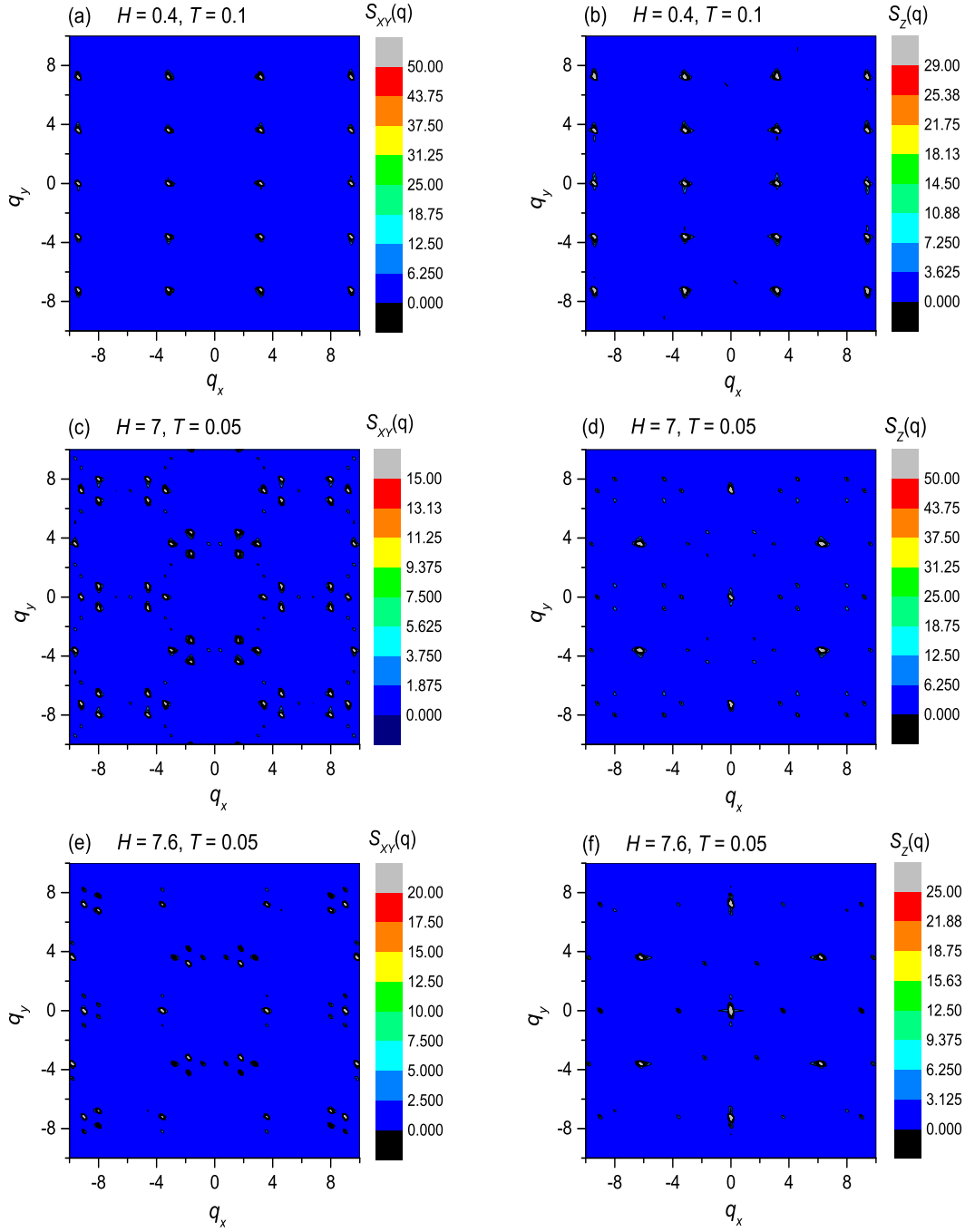


FIG. 8. Intensity patterns of the static spin structure factors for the helical phase at  $H = 0.4$ ,  $T = 1$  (a,b); AF SL phase when  $H = 7$ ,  $T = 0.05$  (c,d), and AF VL phase at  $H = 7.6$ ,  $T = 0.05$  (e,f), respectively.

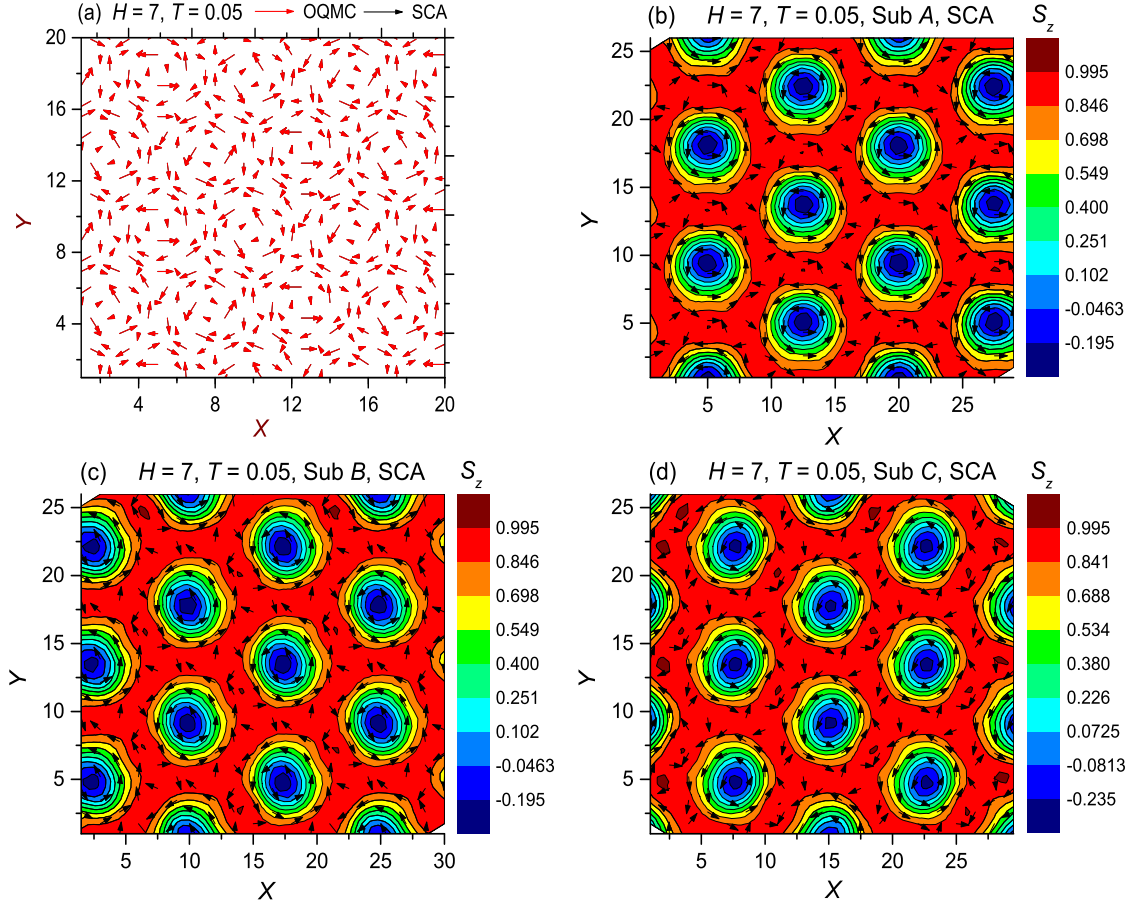


FIG. 9. Calculated (a)  $xy$ -projections, and (b,c,d) three FM sublattices for the AF SLs at  $H = 7$ ,  $T = 0.05$  with the SCA methods.

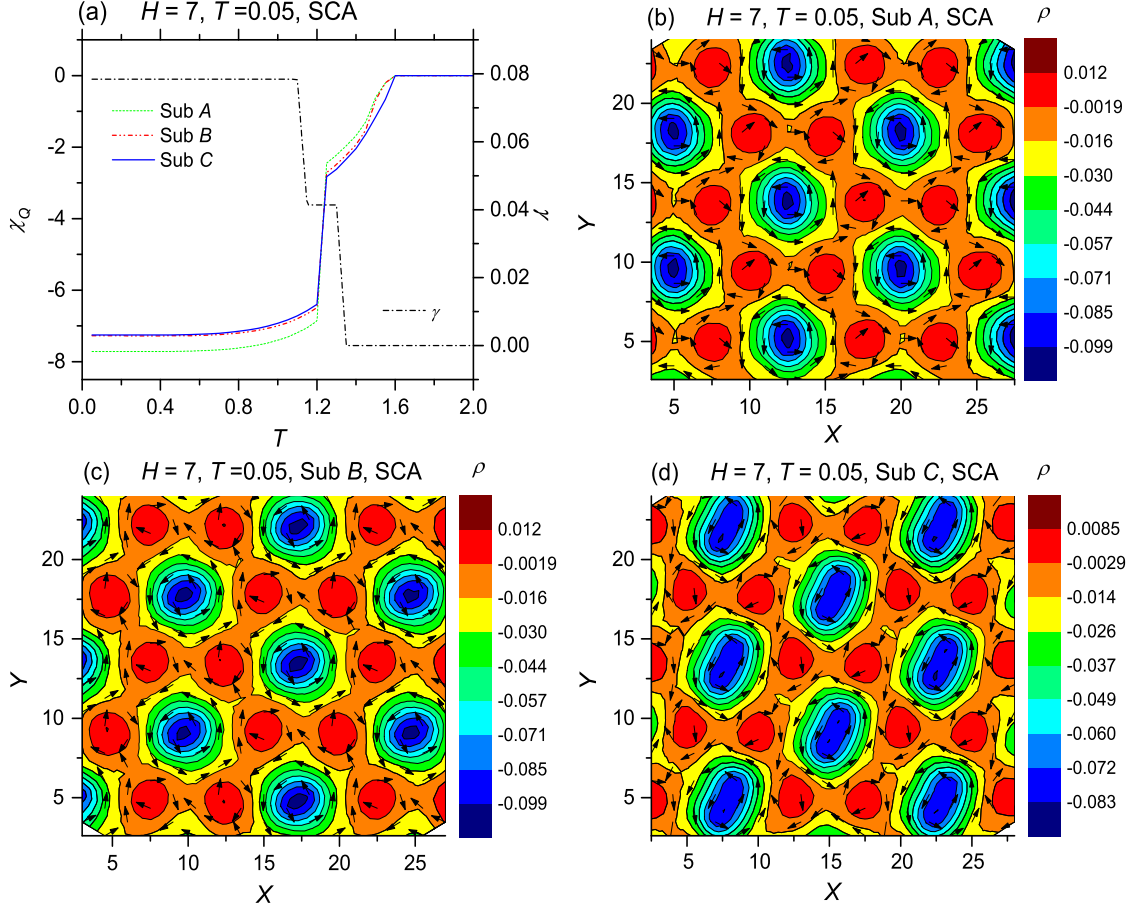


FIG. 10. The total topological charges (a) , and charge density distributions of the three FM sublattices (b,c,d) of the AF SL at  $H = 7$ ,  $T = 0.05$  calculated with the SCA method.

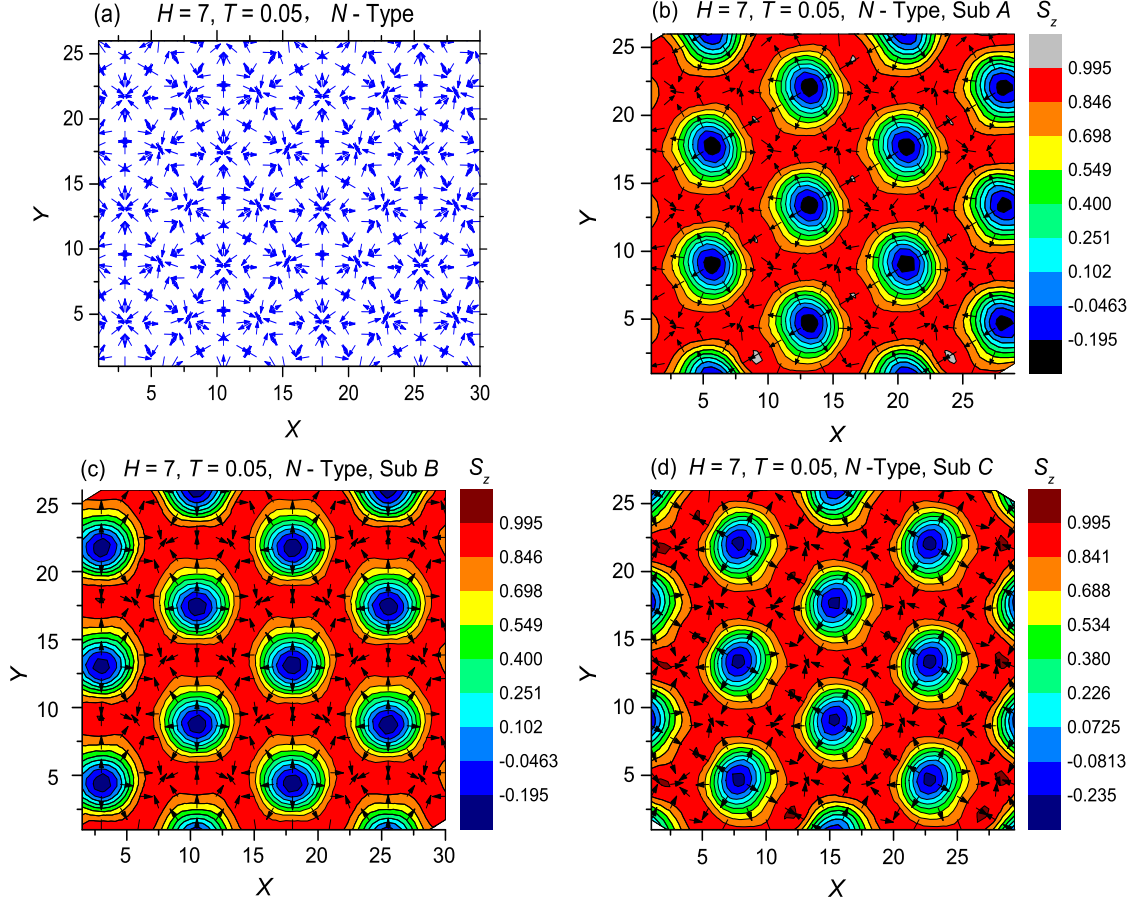


FIG. 11. The  $xy$ -projection (a), and three FM sublattices (b,c,d), of the Néel-type AF SkL calculated with the OQMC method when  $H = 7, T = 0.05$ .

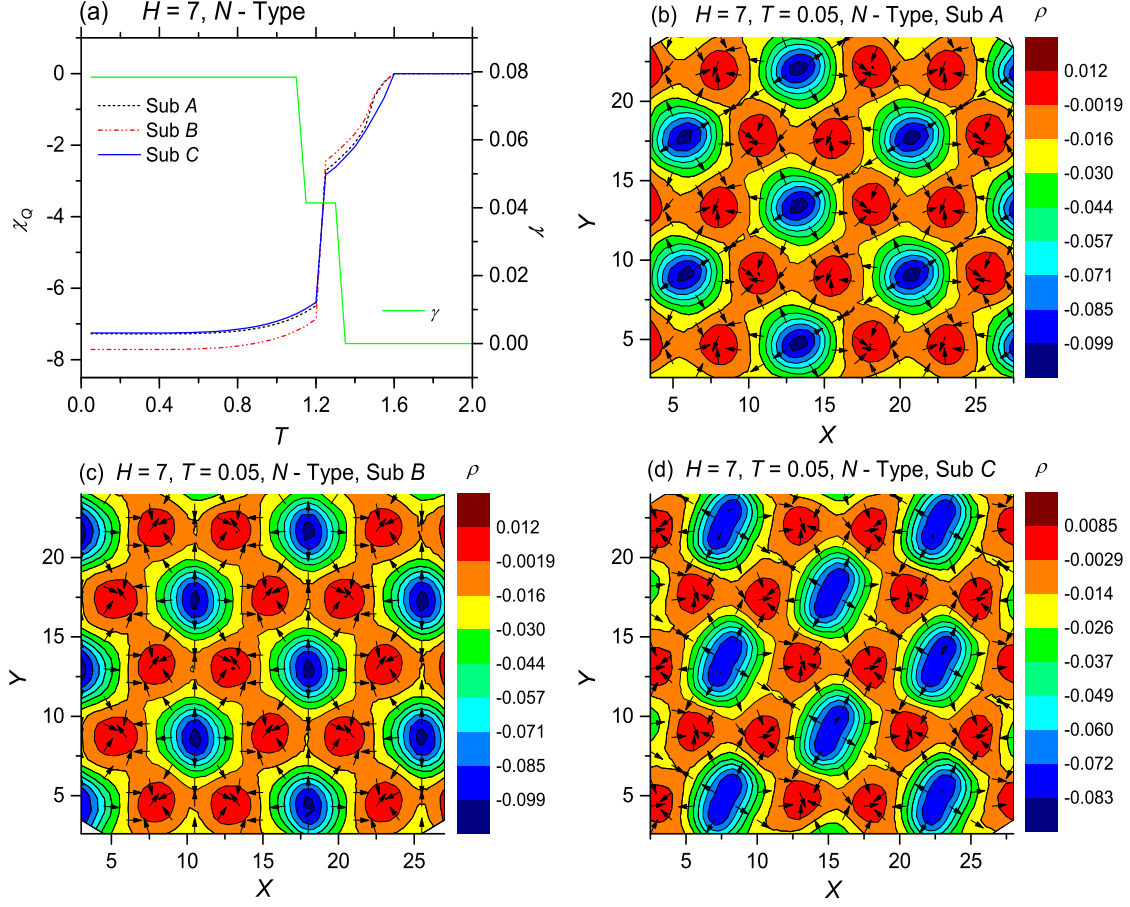


FIG. 12. Total topological charges (a), and charge density distributions of the three FM sublattices (b,c,d), of the Néel-type AFM SkL calculated at  $H = 7$ ,  $T = 0.05$  using the OQMC method.